LA-UR-20-20907 (Accepted Manuscript)

Complete collision data set for electrons scattering on molecular hydrogen and its isotopologues: I. Fully vibrationally-resolved electronic excitation of H

Scarlett, Liam H.
Fursa, D. V.
Zammit, Mark Christian
Bray, I.
Ralchenko, Yuri
Davie, Kayla D

To be published in: Atomic Data and Nuclear Data Tables

DOI to publisher's version: 10.1016/j.adt.2020.101361

Permalink to record: http://permalink.lanl.gov/object/view?what=info:lanl-repo/lareport/LA-UR-20-20907

Atomic Data and Nuclear Data Tables xxx (xxxx) xxx

Contents lists available at ScienceDirect

Atomic Data and Nuclear Data Tables

journal homepage: www.elsevier.com/locate/adt

Complete collision data set for electrons scattering on molecular hydrogen and its isotopologues: I. Fully vibrationally-resolved electronic excitation of $H_2(X\ ^1\Sigma_g^+)$

Liam H. Scarlett [a,*], Dmitry V. Fursa [a], Mark C. Zammit [b], Igor Bray [a], Yuri Ralchenko [c], Kayla D. Davie [d]

[a] Curtin Institute for Computation and Department of Physics and Astronomy, Curtin University, Perth, Western Australia 6102, Australia
[b] Theoretical Division, Los Alamos National Laboratory, Los Alamos, NM 87545, USA
[c] National Institute of Standards and Technology, Gaithersburg, MD 20899-8422, USA
[d] Applied Mathematics & Statistics and Scientific Computation Program, University of Maryland, College Park, MD 20742, USA

ARTICLE INFO

Article history:
Received 27 January 2020
Received in revised form 27 April 2020
Accepted 16 June 2020
Available online xxxx

ABSTRACT

We present a comprehensive set of vibrationally-resolved cross sections for electron-impact electronic excitation of molecular hydrogen suitable for implementation in collisional-radiative models. The adiabatic-nuclei molecular convergent close-coupling method is used to calculate cross sections for excitation of all bound vibrational levels and dissociative excitation of the $B\ ^1\Sigma_u^+$, $C\ ^1\Pi_u$, $EF\ ^1\Sigma_g^+$, $B'\ ^1\Sigma_u^+$, $GK\ ^1\Sigma_g^+$, $I\ ^1\Pi_g$, $J\ ^1\Delta_g$, $D\ ^1\Pi_u$, $H\ ^1\Sigma_g^+$, $b\ ^3\Sigma_u^+$, $c\ ^3\Pi_u$, $a\ ^3\Sigma_g^+$, $e\ ^3\Sigma_u^+$, $d\ ^3\Pi_u$, $h\ ^3\Sigma_g^+$, $g\ ^3\Sigma_g^+$, $i\ ^3\Pi_g$, and $j\ ^3\Delta_g$ electronic states from all $v_i = 0$–14 bound vibrational levels of the ground electronic ($X\ ^1\Sigma_g^+$) state. The data set consists of cross sections from threshold to 500 eV for over 5000 transitions, representing all possible electronic and vibrational transitions between the $X\ ^1\Sigma_g^+$ state and the $n = 2$–3 singlet and triplet states (where n refers to the united-atoms-limit principle quantum number). The cross sections are presented in graphical form and provided as both numerical values and analytic fit functions in supplementary data files. The data can also be downloaded from the MCCC database at http://mccc-db.org.

* Corresponding author.
E-mail address: liam.scarlett@postgrad.curtin.edu.au (L.H. Scarlett).

https://doi.org/10.1016/j.adt.2020.101361
0092-640X/

Please cite this article in press as: L.H. Scarlett, D.V. Fursa, M.C. Zammit et al., Complete collision data set for electrons scattering on molecular hydrogen and its isotopologues: I. Fully vibrationally-resolved electronic excitation of $H_2(X\ ^1\Sigma_g^+)$, Atomic Data and Nuclear Data Tables (2020) 101361, https://doi.org/10.1016/j.adt.2020.101361.

Contents

1. Introduction ... 2
2. Computational details ... 3
2.1. Molecular structure ... 3
2.2. Adiabatic-nuclei calculations ... 4
3. Cross sections and analytic fits ... 5
4. Uncertainty estimates ... 6
5. Accessing the data ... 7
6. Conclusions ... 8
Declaration of competing interest ... 8
Acknowledgment ... 8
Appendix A. Diatomic state notation ... 8
Appendix B. Supplementary data ... 9
References ... 9
Explanation of tables ... 10
Table 1. Vibrational-state energies. ... 10
Explanation of graphs ... 11
Table 2. Dissociative excitation cross sections. ... 11
Table 3. Bound excitation cross sections for the $B\ ^1\Sigma_u^+$ state. ... 11
Table 4. Bound excitation cross sections for the $C\ ^1\Pi_u$ state. ... 11
Table 5. Bound excitation cross sections for the $B'\ ^1\Sigma_u^+$ state. ... 11
Table 6. Bound excitation cross sections for the $a\ ^3\Sigma_g^+$ state. ... 11
Table 7. Bound excitation cross sections for the $c\ ^3\Pi_u$ state. ... 11
Table 8. Bound excitation cross sections for the $d\ ^3\Pi_u$ state. ... 11

1. Introduction

Collisional interactions between electrons and molecules are an important influence on the dynamics of low-temperature plasmas. Measurements of emission spectra can be used to infer the properties of various plasmas and their environments in circumstances where direct observation is unfeasible. For example, spectroscopic measurements of auroral emissions from the giant planets taken from ground-based observatories, Earth-orbiting satellites, and fly-by or orbiting spacecraft are used to determine properties of the magnetospherical plasma as well as details of the atmospheric composition [1]. The aurorae of the outer planets are predominantly related to emissions from atomic and molecular hydrogen [2], and hence detailed knowledge of the various collisional processes for these species is vital to the construction of accurate auroral models.

In fusion plasma diagnostics, a variety of tools such as optical emission or absorption spectroscopy are used to infer the plasma parameters from measurements of spectra and the analyzed population densities [3]. Collisional processes involving the isotopologues of molecular hydrogen will be a major factor in governing the properties and dynamics of the edge and divertor plasmas in the ITER reactor, which in turn will affect the performance of the bulk fusion plasma [4]. Additionally, surface-material damage due to plasma-emission radiation and contact with high-energy particles must be accounted for when designing reactor components. The plasma-facing components of the divertor are subject to a particularly strong heat load, and there is considerable interest in understanding the influence of molecular species on the behavior of the divertor plasma due to their crucial role in the detached divertor regime, which is characterized by a significant reduction in plasma temperature and particle flux at the divertor targets [5,6]. Reliable plasma diagnostics for both ionizing and recombining plasmas are also important for improving the efficiency and minimizing wear on the beam-line components of the negative-ion neutral-beam-injection (N-NBI) system, which will be one of the primary external heating mechanisms at ITER [7]. Although ITER will eventually operate with a deuterium–tritium fuel cycle, the preliminary phases of operation will employ hydrogen and deuterium fuel cycles, and hence data for each of the H_2, D_2, and T_2 molecules will be necessary.

The essential tool for relating emission spectra to the underlying plasma properties is the collisional-radiative (CR) model. CR models balance the competing excitation and de-excitation processes, ionization and recombination processes, and association and dissociation processes to determine the steady-state population densities of the plasma species, and hence require comprehensive sets of collision data for the species of interest [8]. Accurate electron-impact cross section data are critically important for implementation in CR models. Raw cross section data as a function of energy is also necessary for the calculation of transport and rate coefficients using Boltzmann solvers (such as BOLSIG+) [9]. Currently, there are several reliable CR models for highly-ionized plasmas, where the perturbative electron-scattering approaches (e.g. distorted-wave or Coulomb–Born) are suitable [10,11], and general suites of codes exist [12–15] (and references therein). The situation is somewhat different for near-neutral plasmas, where only a number of complete sets of accurate collision data exist for near-neutral atomic species (e.g. hydrogen, helium, beryllium and argon) [16–19]. Even more difficulties arise due the presence of molecules in near-neutral plasmas.

The collision data available for molecular species is much less comprehensive than for atomic species. Even for the simplest neutral molecule H_2, there are at present no available sets of collision data which include rovibrational sublevels, transitions between excited states, and isotope effects. Two widely-used sets of collision data that have been utilized in previous CR models are those of Janev et al. [20] and Miles et al. [21], both representing data inferred from various experimental or theoretical sources. For many transitions in H_2 the two data sets are in significant disagreement, in some cases differing by an order of magnitude. This is an unsatisfactory situation from the perspective of CR modeling as inconsistent input data leads to highly unreliable diagnostics. There are 5 isoelectronic variants of H_2, with the deuterated and triterated isotopologues being of particular importance for fusion. The collision data sets available for the isotopologues are significantly worse than for H_2. Even for D_2 very little data is available [22].

Please cite this article in press as: L.H. Scarlett, D.V. Fursa, M.C. Zammit et al., Complete collision data set for electrons scattering on molecular hydrogen and its isotopologues: I. Fully vibrationally-resolved electronic excitation of $H_2(X\ ^1\Sigma_g^+)$, Atomic Data and Nuclear Data Tables (2020) 101361, https://doi.org/10.1016/j.adt.2020.101361.

The most comprehensive set of calculated cross sections to date was generated using the semi-classical impact-parameter (IP) method for excitation of the singlet electronic states from the ground electronic ($X\ ^1\Sigma_g^+$) state, and the Gryzinski approximation for excitation of the dissociative $b\ ^3\Sigma_u^+$ state [23] (see Appendix A for a description of the molecular-state notation). Comparison with more recent molecular convergent close-coupling (MCCC) calculations [24] has shown that these results are inaccurate at low to intermediate energies (up to a factor of two too large at the cross section maximum). Furthermore, the dataset of Ref. [23] does not account for excitation of triplet states above the $b\ ^3\Sigma_u^+$ state.

The development of the MCCC method in recent years and its application to electrons scattering on H_2 allows for an updated set of cross sections to be produced which improves upon the previously available data in both the accuracy of the cross sections and the number of included transitions. Detailed convergence studies for e^--H_2 scattering have previously been performed with a spherical-coordinate implementation of the MCCC method [25], representing the first explicit demonstration of convergence in electron–molecule scattering, and resulting in a set of cross sections for electronic excitation and ionization from the ground (electronic and vibrational) state of H_2. The accuracy of the MCCC results is supported by the excellent agreement with recent measurements of the $X\ ^1\Sigma_g^+(v_i = 0) \rightarrow b\ ^3\Sigma_u^+$ excitation [26,27], the most fundamental electronic transition in e^--H_2 scattering for which the agreement between previous calculations and measurements was particularly poor. A spheroidal-coordinate formulation of the MCCC method has also been developed, with the aim of studying scattering from excited vibrational levels. We have implemented a spheroidal structure and scattering model which yields convergent cross sections for the low-lying electronic transitions [28], and have applied it to studies of a number of excitation and dissociation processes [24,29–31].

The present aim of the MCCC project is to produce a complete set of state-to-state electron-impact collision data for H_2 and its isotopologues, including fully vibrationally-resolved electronic excitation and ionization for scattering on vibrationally-excited levels of the ground ($X\ ^1\Sigma_g^+$) and excited electronic states. We hope the MCCC results will resolve the long-standing issues of inaccurate or incomplete e^--H_2 collision data and aid in the construction of reliable CR models. The first contribution to the data set, which we outline in this paper, is a set of fully vibrationally-resolved electronic excitation cross sections for scattering on the $v_i = 0$–14 vibrational levels of the $X\ ^1\Sigma_g^+$ state of H_2 to all vibrational levels in each state of the $n = 2$ and $n = 3$ singlet and triplet spectra. Cross sections for dissociative excitation (DE) of each of these states are also included. Data for the deuterated and triterated isotopologues, including excitation, ionization, viscosity, and momentum transfer cross sections, will be provided in future contributions to the data set. Atomic units are used throughout this paper, except where specified otherwise.

2. Computational details

In this section we briefly outline the present MCCC calculations, and provide references for previous publications where the interested reader can find in-depth discussions of the MCCC theory and details of the structure and scattering models we have implemented.

2.1. Molecular structure

The structure calculations are performed in the molecular body frame using prolate spheroidal coordinates, with the internuclear axis aligned with the z axis and the nuclei placed at the two focii. Neglecting rotational motion, the molecular target states are represented in the Born–Oppenheimer approximation as products of electronic and vibrational wave functions:

$$\Phi_{nv}(\mathbf{x_1}, \mathbf{x_2}, R) = \Phi_n(\mathbf{x_1}, \mathbf{x_2}; R)\nu_{nv}(R), \quad (1)$$

where v denotes a vibrational level in the electronic state n, $\mathbf{x_1}$ and $\mathbf{x_2}$ are the target-electron spatial and spin coordinates, and R is the internuclear separation. The use of spheroidal coordinates allows the electronic wave functions Φ_n to be calculated accurately over the range of R values spanned by all $v_i = 0$–14 bound vibrational levels of the ground electronic ($X\ ^1\Sigma_g^+$) state. For explicit details of the structure calculation utilized in the present work see Ref. [28]. In Table A we present the two-electron energies for the electronic states under present consideration at the equilibrium separation $R = 1.4\ a_0$, and compare with accurate structure calculations from the literature [32–37]. In Figs. 1 and 2 we present the energies as a function of internuclear separation, compared with the accurate potential energy curves obtained from Refs. [32–37].

Table A
Two-electron energy of electronic states of H_2 at the internuclear distance $R = 1.4\ a_0$. Comparison is made with accurate structure calculations from the literature [32–37].

	State	Energy (Ha)	
		Present	Ref.
Singlets	$X\ ^1\Sigma_g^+$	−1.1710	−1.1745 [32]
	$B\ ^1\Sigma_u^+$	−0.7047	−0.7058 [33]
	$EF\ ^1\Sigma_g^+$	−0.6914	−0.6920 [34]
	$C\ ^1\Pi_u$	−0.6881	−0.6887 [35]
	$B'\ ^1\Sigma_u^+$	−0.6283	−0.6287 [33]
	$GK\ ^1\Sigma_g^+$	−0.6263	−0.6265 [34]
	$I\ ^1\Pi_g$	−0.6260	−0.6262 [36]
	$J\ ^1\Delta_g$	−0.6251	−0.6253 [36]
	$H\ ^1\Sigma_g^+$	−0.6241	−0.6244 [34]
	$D\ ^1\Pi_u$	−0.6234	−0.6236 [35]
Triplets	$b\ ^3\Sigma_u^+$	−0.7835	−0.7842 [37]
	$a\ ^3\Sigma_g^+$	−0.7133	−0.7136 [37]
	$c\ ^3\Pi_u$	−0.7060	−0.7066 [37]
	$e\ ^3\Sigma_u^+$	−0.6435	−0.6435 [37]
	$h\ ^3\Sigma_g^+$	−0.6301	−0.6303 [37]
	$d\ ^3\Pi_u$	−0.6286	−0.6288 [37]
	$g\ ^3\Sigma_g^+$	−0.6263	−0.6266 [37]
	$i\ ^3\Pi_g$	−0.6260	−0.6262 [37]
	$j\ ^3\Delta_g$	−0.6252	−0.6253 [36]

The vibrational wave functions ν_{nv} in Eq. (1) are the eigenstates of the Born–Oppenheimer vibrational Hamiltonian. We assume a Hund's case (b) coupling scheme, where the rotational levels are indexed by the quantum number N of the total angular momentum without spin, and the vibrational Hamiltonian is given by [38]

$$H_n^{\mathrm{BO}} = -\frac{1}{2\mu}\frac{\mathrm{d}^2}{\mathrm{d}R^2} + \frac{N(N+1) - \Lambda_n^2}{2\mu R^2} + \epsilon_n(R), \quad (2)$$

where μ is the nuclear reduced mass, Λ_n is the electronic orbital angular momentum projection of the state n onto the internuclear axis, and ϵ_n is the potential energy curve of the electronic state n.

For low rotational quantum numbers, the centrifugal term in Eq. (2) is negligible compared to the potential-energy term, and hence we neglect it.

The vibrational wave functions are obtained by diagonalizing Eq. (2) in a basis of Sturmian (Laguerre) functions. The number of basis functions is chosen to yield convergent energies in the bound spectrum and an adequate discretization of the vibrational continuum. In Table B we summarize the number of bound vibrational levels in each electronic state, and in Table 1 we compare

Please cite this article in press as: L.H. Scarlett, D.V. Fursa, M.C. Zammit et al., Complete collision data set for electrons scattering on molecular hydrogen and its isotopologues: I. Fully vibrationally-resolved electronic excitation of $H_2(X\ ^1\Sigma_g^+)$, Atomic Data and Nuclear Data Tables (2020) 101361, https://doi.org/10.1016/j.adt.2020.101361.

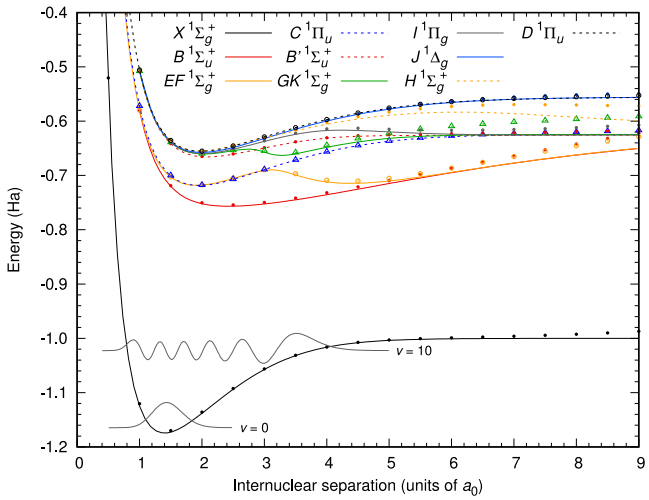

Fig. 1. Potential energy curves from the present spheroidal structure calculation for the singlet states of H_2 (symbols), compared with accurate energies from the literature (lines). References for the literature values are as stated in Table A. Also presented are the $v = 0$ and $v = 10$ vibrational wave functions in the $X\,^1\Sigma_g^+$ state.

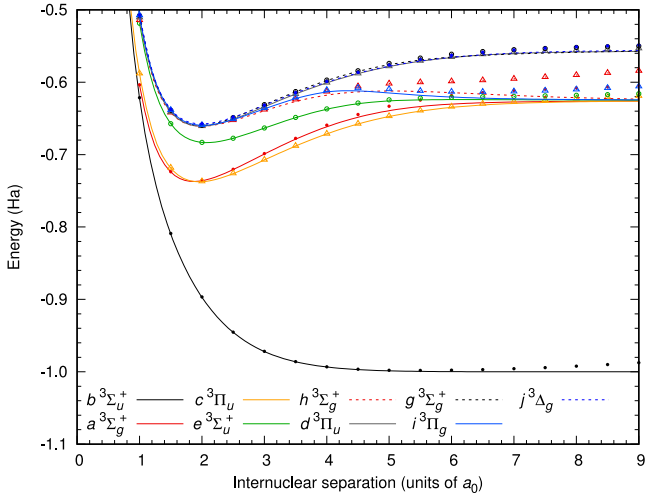

Fig. 2. Same as in Fig. 2 but for the triplet states of H_2.

the present vibrational-state energies with the calculations of Fantz and Wünderlich [39]. To limit the size of the table we present energies for a maximum of 15 levels in each electronic state, with the full set of energies available in the supplementary material. Vibrational levels with wave functions located in the outer well of a double-minima state are marked with an asterisk. For the $H\,^1\Sigma_g^+$ state the inner/outer well sequence of the vibrational wave functions differs slightly between our calculations and Ref. [39] (here $v = 8$ and 13 are located in the inner well while in Ref. [39] they are in the outer well). We note that our assignment of the $v = 8$ and 13 levels to the inner well is in agreement with the calculations of Ross et al. [40].

2.2. Adiabatic-nuclei calculations

The adiabatic-nuclei (AN) MCCC method has been described in detail in Refs. [24,41], so only a brief outline will be given here.

The Born–Oppenheimer approximation is applied to the total scattering wave function:

$$\Psi_{iv_i}(\mathbf{x_0}, \mathbf{x_1}, \mathbf{x_2}, R) = \Psi_i(\mathbf{x_0}, \mathbf{x_1}, \mathbf{x_2}; R)\nu_{iv_i}(R), \tag{3}$$

Table B
The number of bound vibrational levels in each of the electronic states of H_2 under consideration in the present work.

Singlets		Triplets	
State	N_{bound}	State	N_{bound}
$X\,^1\Sigma_g^+$	15	$b\,^3\Sigma_u^+$	0 (dissociative)
$B\,^1\Sigma_u^+$	40	$a\,^3\Sigma_g^+$	22
$EF\,^1\Sigma_g^+$	33	$c\,^3\Pi_u$	22
$C\,^1\Pi_u$	14	$e\,^3\Sigma_u^+$	8
$B'\,^1\Sigma_u^+$	10	$h\,^3\Sigma_g^+$	4
$GK\,^1\Sigma_g^+$	9	$d\,^3\Pi_u$	21
$I\,^1\Pi_g$	9	$g\,^3\Sigma_g^+$	20
$J\,^1\Delta_g$	19	$i\,^3\Pi_g$	4
$H\,^1\Sigma_g^+$	72	$j\,^3\Delta_g$	19
$D\,^1\Pi_u$	19		

where $\mathbf{x_0}$ are the projectile spatial and spin coordinates. This allows the electronic scattering problem to be solved independently for each value of R. We have implemented a close-coupling expansion consisting of 210 bound and continuum (ionization) pseudostates. The accuracy of the structure model ensures that the low-lying target states are good representations of the true spectroscopic states, while the remaining pseudostates provide an adequate representation of the higher-energy bound states and a discretization of the ionization continuum.

Once the electronic scattering calculations have been conducted at a suitable number of R points, the dependence on the nuclear motion is reintroduced with the AN approximation, yielding cross sections for vibrationally-resolved transitions $iv_i \to fv_f$:

$$\sigma_{fv_f,iv_i}(E_{\text{in}}) = \frac{q_f}{4\pi q_i} \sum_{\substack{L_f,L_i \\ M_f,M_i}} \left|\langle \nu_{fv_f} | F_{fL_fM_f,iL_iM_i}(R; E_{\text{in}}) | \nu_{iv_i}\rangle\right|^2, \tag{4}$$

where q_f and q_i are the projectile outgoing and incident momenta, respectively, E_{in} is the projectile incident energy, and $F_{fL_fM_f,iL_iM_i}$ are the fixed-nuclei partial-wave scattering amplitudes for the $i \to f$ transition. In Eq. (4) the cross sections have been analytically summed over final rotational levels (see Ref. [41] for details).

Directly evaluating Eq. (4) can lead to significant instabilities in the vibrationally-resolved cross sections for a few reasons. The FN cross sections can be affected by pseudoresonances or numerical irregularities (see Ref. [28] for examples), interpolation of the amplitudes per partial-wave can be much more difficult than interpolating the FN cross sections over R, and the breakdown of the adiabatic approximation at near threshold energies can lead to unusual behavior as the R-dependent thresholds of the fixed-nuclei amplitudes are approached. In the present calculations we have applied the "square-root" approximation

$$\sigma_{fv_f,iv_i}(E_{\text{in}}) \approx \left|\langle \nu_{fv_f} | \sqrt{\sigma_{f,i}(R; E_{\text{in}})} | \nu_{iv_i}\rangle\right|^2, \tag{5}$$

which requires only the FN cross sections to be interpolated over R at each energy, rather than each individual partial-wave amplitude. We have applied this approximation previously [42,43] and found that it produces results which are practically identical to the true AN cross sections. By comparing with results obtained from direct evaluation of Eq. (4) we have confirmed that the approximation is similarly accurate in the present calculations at above-threshold energies, but produces smoother cross sections near excitation thresholds.

At low energies there is a threshold value of R in the FN cross sections, leading to the unphysical situation where $\sigma_{f,i}(R; E_{\text{in}})$ is zero for a portion of the integration in Eq. (5) (see Fig. 8 of Ref. [44] for an example of this). The change of the threshold

Please cite this article in press as: L.H. Scarlett, D.V. Fursa, M.C. Zammit et al., Complete collision data set for electrons scattering on molecular hydrogen and its isotopologues: I. Fully vibrationally-resolved electronic excitation of $H_2(X\,^1\Sigma_g^+)$, Atomic Data and Nuclear Data Tables (2020) 101361, https://doi.org/10.1016/j.adt.2020.101361.

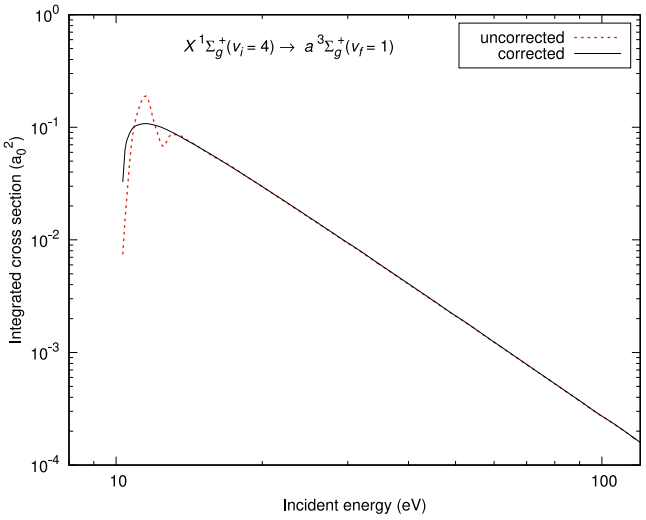

Fig. 3. Comparison of cross sections for the $X\ ^1\Sigma_g^+(v_i = 4) \rightarrow a\ ^3\Sigma_g^+(v_f = 1)$ transition with and without the energy-balancing correction discussed in the text.

R value as the incident energy is varied can produce undesired oscillations in the vibrationally-resolved cross sections. This difficulty is a result of a larger problem with the AN method: the FN collision data used in Eqs. (4)–(5) do not satisfy energy-conservation requirements because the FN outgoing momentum is a function of the vertical excitation energy only, rather than depending on the specific vibrational transition. Shugard and Hazi [45] proposed a remedy to this issue which requires the use of off-shell scattering amplitudes (off the energy shell in the FN formalism) to ensure that both the incoming and outgoing projectile momenta used to obtain the FN amplitude are correct for each vibrational transition and that the FN transition is open at all values of R. Stibbe and Tennyson [46] developed a simpler "energy-balancing" correction which still ensures that the outgoing momentum is correct, but varies the incident energy with R:

$$E_{f v_f, i v_i}(R; E_{\rm in}) = E_{\rm in} - \varepsilon_{f v_f, i v_i} + \epsilon_{f,i}(R), \tag{6}$$

so that only on-shell FN collision data are required. Although this method was initially developed to study dissociative excitation, we have adopted a similar approach here, and evaluate cross sections for both bound and dissociative transitions using

$$\sigma_{f v_f, i v_i}(E_{\rm in}) = \left| \langle \nu_{f v_f} | \sqrt{\sigma_{f,i}(R, E_{f v_f, i v_i}(R; E_{\rm in}))} | \nu_{i v_i} \rangle \right|^2 . \tag{7}$$

Cross sections for dissociative excitation are obtained by summing Eq. (7) over the vibrational continuum pseudostates obtained from diagonalizing Eq. (2) (see Ref. [29] for details). In Fig. 3 we compare the cross sections for excitation of the $X\ ^1\Sigma_g^+(v_i = 4) \rightarrow a\ ^3\Sigma_g^+(v_f = 1)$ transition calculated with and without the energy-balancing correction. At lower energies there are oscillations in the uncorrected cross section which are not present in the corrected cross section.

We have performed calculations using the MCCC(210) model with 20 R points between 0.8 and 8.0 a_0 for 10 energies between 10 and 40 eV. At 60, 80, and 120 eV we have used fewer R points (8 between 0.8 and 8.0 a_0) as there is less variation in the R-dependent cross sections at higher energies. The MCCC(210) model is sufficient to yield convergent cross section for the discrete transitions we consider in this work [28] but is computationally expensive, requiring approximately 10,000 cpu hours per energy and internuclear separation. In addition to the MCCC(210) model, we have also run calculations using a model consisting of 27 bound electronic states (neglecting ionization channels) on finer energy and R grids: 25 energies between 1 and 40 eV and an additional 25 energies up to 500 eV, each with 25 R points between 0.8 and 8.0 a_0. We have shown previously that the MCC(27) model is sufficiently convergent above 120 eV [24,30] so we use these results to extend the MCCC(210) cross sections up to 500 eV. We require results down to 1 eV for the $X\ ^1\Sigma_g^+ \rightarrow b\ ^3\Sigma_u^+$ transition, which at these energies is converged even with a 12-state model [44] so here the MCC(27) model is also sufficient. In order to increase the density of energy and R points in the MCCC(210) calculations between 10 and 120 eV, we utilize a procedure where cross sections from the MCC(27) model are scaled as a function of energy and R to fit the MCCC(210) results. We have demonstrated the reliability of this approach previously [24].

In order to obtain reliable AN cross sections we have found it necessary to ensure that the FN cross sections at each value of R are a smooth function of energy. We have shown previously that when evaluating AN cross sections summed over final vibrational levels the instabilities in the FN cross sections largely disappear [28], however specific vibrational transitions can be much more sensitive to variations in the FN collision data. In order to produce a set of smooth FN cross sections for use in the AN calculations we have adopted an approach where analytic functions are fitted to the FN cross sections for each value of R, before recompiling them as a set of R-dependent cross sections at each incident energy. The analytic functions we utilized in this step are similar in form to those described in the following section to fit to the vibrationally-resolved cross sections, and by comparing AN calculations performed using the raw FN cross sections with those performed using the fitted cross sections we have confirmed that aside from removing irregularities in the final results this procedure has no substantial effect on the overall shape and magnitude of the cross sections.

3. Cross sections and analytic fits

Cross sections have been calculated for all possible transitions between the v_i = 0–14 vibrational levels of the ground electronic ($X\ ^1\Sigma_g^+$) state and all bound vibrational levels of the excited electronic states listed in Table B. Dissociative excitation cross sections have also been obtained for each excited electronic state. For the direct transitions we have performed calculations from threshold up to 500 eV, while for the exchange The lowest-lying excited state ($b\ ^3\Sigma_u^+$) is purely repulsive within the Franck–Condon region of the $X\ ^1\Sigma_g^+$ state and hence only dissociative excitation is possible. There are over 5000 transitions in the present data set, and hence we do not tabulate the cross sections here. Instead, we present a subset of example data in graphical form: in Graph 1 we present DE cross sections for the $B\ ^1\Sigma_u^+$, $C\ ^1\Pi_u$, $B'\ ^1\Sigma_u^+$, $b\ ^3\Sigma_u^+$, $a\ ^3\Sigma_g^+$, and $c\ ^3\Pi_u$ states, and in Graphs 2–7 we present bound-excitation cross sections for a selection of vibrational transitions between the $X\ ^1\Sigma_g^+$ state and the $B\ ^1\Sigma_u^+$, $C\ ^1\Pi_u$, $B'\ ^1\Sigma_u^+$, $a\ ^3\Sigma_g^+$, $c\ ^3\Pi_u$, and $d\ ^3\Pi_u$ states. All of the cross sections are available in text files as outlined in Section 5.

In addition to numerical cross sections, we also provide analytic fits for each transition. For excitation of the singlet states, we have employed the following analytic function:

$$\sigma(x) = \left| \frac{x-1}{x} \cdot \left(\frac{a_0^2}{x} \ln x + \frac{a_1}{x} + \frac{a_2}{x^2} + \frac{a_3}{x^3} + \frac{a_4}{x^4} + \frac{a_5}{x^5} \right) \right| . \tag{8}$$

Here, $x = E_{\rm in}/E_0$, where E_0 is the threshold energy. For excitation of the triplet states above the $b\ ^3\Sigma_u^+$ state, we use

$$\sigma(x) = \left| \frac{x-1}{x} \cdot \left(\frac{a_0^2}{x} + \frac{a_1}{x^2} + \frac{a_2}{x^3} + \frac{a_3}{x^4} + \frac{a_4}{x^5} \right) \right| . \tag{9}$$

Please cite this article in press as: L.H. Scarlett, D.V. Fursa, M.C. Zammit et al., Complete collision data set for electrons scattering on molecular hydrogen and its isotopologues: I. Fully vibrationally-resolved electronic excitation of $H_2(X\ ^1\Sigma_g^+)$, Atomic Data and Nuclear Data Tables (2020) 101361, https://doi.org/10.1016/j.adt.2020.101361.

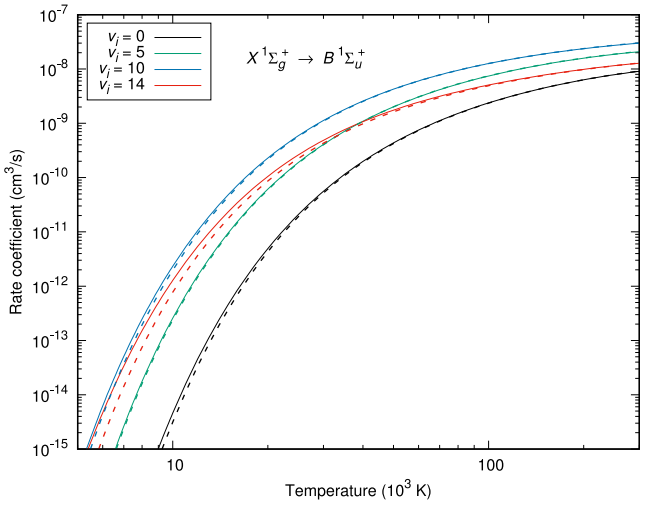

Fig. 4. Rate coefficients summed over final vibrational levels for excitation of the $B\,^1\Sigma_u^+$ state from the $v_i = 0$, 5, 10, and 14 vibrational levels of the $X\,^1\Sigma_g^+$. The solid lines are calculations performed using the numerical MCCC cross sections, while the dashed lines are calculations performed using the fitted cross sections.

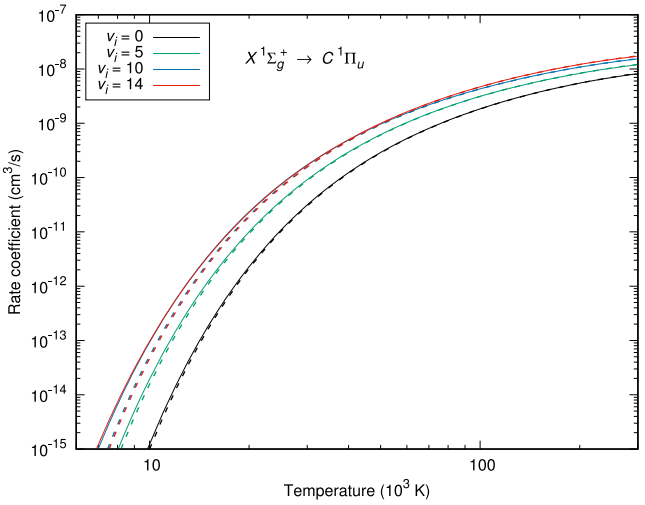

Fig. 5. Same as in Fig. 4 but for excitation of the $C\,^1\Pi_u$ state.

These two functions provide adequate fits for both the bound and dissociative excitations. For the $b\,^3\Sigma_u^+$ state, we use a different form:

$$\sigma(x) = a_0(x-1)^{-a_1^2}\exp\left[-\frac{a_2}{(x-1)^{a_3}}\right]. \quad (10)$$

The distribution of the cross section for an electronic transition $i \rightarrow f$ over the various vibrational levels in the upper electronic state f can often lead to large differences of an order of magnitude or more between the stronger and weaker vibrational transitions. In these cases the cross sections of small magnitude tend to be numerically unstable. We expect this will have no effect in applications of the collision data as any instabilities in the small cross sections are masked by the larger cross sections.

However, fitting the analytic functions (8)–(9) to these cross sections can be difficult and in some instances leads to slightly negative cross sections in the near-threshold region due to spurious oscillations in the fitting functions.

These oscillations are insignificant in magnitude, but to avoid potential errors caused by modeling codes expecting non-negative cross sections we have included the absolute-value signs in Eqs. (8) and (9) to guarantee a positive cross section at all energies.

In order to illustrate the accuracy of the analytic fits in a practical application, we have calculated and compared rate coefficients

$$c_{f v_f, i v_i} = \frac{8\pi}{m_e^{1/2}}\left(\frac{1}{2\pi k_B T}\right)^{3/2}\int_0^\infty \sigma_{f v_f, i v_i}(E_{in}) e^{-E_{in}/k_B T} E_{in}\, dE_{in} \quad (11)$$

using both the numerical and fitted cross sections as input. In Figs. 4 and 5 we present rate coefficients for excitation of the $B\,^1\Sigma_u^+$ and $C\,^1\Pi_u$ states from the $v_i = 0$, 5, 10, and 14 vibrational levels of the $X\,^1\Sigma_g^+$. The calculations were performed for each final vibrational level and summed to produce an overall rate coefficient for the electronic excitation. The rate coefficients calculated using the fitted cross sections are in good agreement with those obtained using the numerical MCCC cross sections.

4. Uncertainty estimates

The three major sources of uncertainty in the present results are the target-structure accuracy, the level of convergence in the FN scattering calculations, and the use of the AN approximation. Detailed convergence studies were presented in a previous publication of fixed-nuclei (FN) electron–H_2 cross sections obtained using the spherical-coordinate MCCC method at the mean internuclear separation of $R = 1.448\ a_0$ [25]. The uncertainty due to convergence was estimated to be better than 5% across all electronic transitions. More recently [28], we have compared the FN cross sections from the present spheroidal-coordinate calculations, and found generally very good agreement with the spherical-coordinate results, with differences for some transitions associated with the more accurate target states in the spheroidal-coordinate structure model. Hence, we estimate a similar 5% uncertainty due to convergence. Although this analysis was performed at $R = 1.448\ a_0$ only, we note that the rate of convergence generally improves at large internuclear separations where the electronic excitation energies become smaller.

The accuracy of the present structure calculation has been demonstrated in Figs. 1 and 2. We find very good agreement with the accurate calculations for the internuclear separations spanned by the $v_i = 0$–10 vibrational levels in the $X\,^1\Sigma_g^+$ state ($R \leq 5.0\ a_0$), with errors generally less than 5% for the larger R values spanned by the remaining $v_i = 11$–14 levels ($R \leq 8.0\ a_0$). The excitation energy $\epsilon_{f,i} = \epsilon_f - \epsilon_i$ is a good indicator of the structure accuracy and its effects on the accuracy of the scattering cross sections. In order to give an overall estimate of the uncertainty in the transitions from an initial vibrational level v_i in the $X\,^1\Sigma_g^+$ state to an excited electronic state f, we can average the relative error in the excitation energy over the v_i vibrational wave function, giving:

$$u_{f,iv_i}^{\text{struc.}} = \langle \nu_{iv_i} \left| \frac{\epsilon_{f,i} - \epsilon_{f,i}^{\text{exact}}}{\epsilon_{f,i}^{\text{exact}}} \right| \nu_{iv_i} \rangle, \quad (12)$$

where $\epsilon_{f,i}$ is the excitation energy from the present structure calculations, and $\epsilon_{f,i}^{\text{exact}}$ is the "exact" excitation energy obtained using the accurate potential-energy curves from Refs. [32–37]. We have found that the uncertainties obtained from Eq. (12) are less than 1% for all initial vibrational levels, so for simplicity we estimate an overall uncertainty of 6% (including the 5% from convergence). We emphasize that this is only an approximate error analysis, and so to avoid giving the impression that the 6% figure is a precise statement of the uncertainty we round up and provide a final uncertainty of 10% in the MCCC H_2 cross sections. In doing so we also hope to cover any additional sources of error such as choices of integration grids, general numerical instabilities, and the use of the AN approximation.

Please cite this article in press as: L.H. Scarlett, D.V. Fursa, M.C. Zammit et al., Complete collision data set for electrons scattering on molecular hydrogen and its isotopologues: I. Fully vibrationally-resolved electronic excitation of $H_2(X\,^1\Sigma_g^+)$, Atomic Data and Nuclear Data Tables (2020) 101361, https://doi.org/10.1016/j.adt.2020.101361.

```
# MCCC calculations of electron scattering on molecular hydrogen
# Adiabatic nuclei calculations performed with the spheroidal MCCC(210) model
# Reference:  Scarlett et al., Atom.  Data Nucl.  Data Tables (2020)
# MCCC Database:  mccc-db.org
# This file:  e + H2(X1Sg,vi=0) -> e + H2(Bp1Su) (dissociative excitation)
# Initial-state energy:  -1.16453 Hartrees
#
# Threshold:  1.46815E+01 eV
#
# Energy (eV)   CS (a_0^2)
  1.46815E+01   0.00000E+00
  1.50000E+01   1.66274E-04
  1.55000E+01   1.49650E-03
  1.60000E+01   3.46034E-03
  1.65000E+01   5.68862E-03
  1.70000E+01   8.00076E-03
  1.75000E+01   1.03085E-02
  1.80000E+01   1.25784E-02
  1.85000E+01   1.47952E-02
  1.90000E+01   1.69492E-02
  1.95000E+01   1.90362E-02
  2.00000E+01   2.10576E-02
  2.10000E+01   2.49076E-02
  2.20000E+01   2.85040E-02
  2.30000E+01   3.18639E-02
  2.40000E+01   3.49997E-02
  2.50000E+01   3.79261E-02
  2.60000E+01   4.06578E-02
  2.70000E+01   4.32065E-02
  2.80000E+01   4.55861E-02
  2.90000E+01   4.78068E-02
  3.00000E+01   4.98836E-02
  3.50000E+01   5.83584E-02
  4.00000E+01   6.44129E-02
  4.50000E+01   6.86708E-02
  5.00000E+01   7.16277E-02
  6.00000E+01   7.48725E-02
  7.00000E+01   7.58857E-02
  8.00000E+01   7.56072E-02
  9.00000E+01   7.45754E-02
  1.00000E+02   7.31118E-02
  1.25000E+02   6.86458E-02
  1.50000E+02   6.39901E-02
  2.00000E+02   5.56524E-02
  2.50000E+02   4.89227E-02
  3.00000E+02   4.35372E-02
  3.50000E+02   3.91795E-02
  4.00000E+02   3.55968E-02
  4.50000E+02   3.25974E-02
  5.00000E+02   3.00624E-02
```

Fig. 6. The format of the file `MCCC-el-H2-Bp1Su_DE.X1Sg_vi=0.txt`, containing the numerical MCCC cross-section for dissociative excitation (DE) of the $B'\ ^1\Sigma_u^+$ state from the $X\ ^1\Sigma_g^+(v_i = 0)$ state of H_2. The threshold energy for each transition can be extracted from the file header.

It is well-known that the AN approximation breaks down at low incident energies, and is unable to describe resonant scattering processes. In the present work we make no attempt to map out resonances in the cross sections. It is difficult to quantitatively assess the uncertainty contributed by the AN approximation until more accurate vibrational close-coupling calculations have been performed, but since the break-down of the approximation occurs at low incident energies where the uncertainty due to convergence is much smaller we expect that the error of 10% quoted above will be sufficient. The various steps discussed in Section 2.2 to improve the AN cross sections, aside from removing unwanted oscillations and instabilities in the cross sections, do not have any substantial effect compared to the sources of error mentioned above.

We now turn to the error in the fitted cross sections. In order to construct an overall uncertainty for each final electronic state we sum the numerical cross sections over the final vibrational levels and compare with the same quantity obtained from the fitted cross sections, giving the relative error in the fitting procedure:

$$u^{\rm fit}_{f,iv_i}(E_{\rm in}) = \left| \frac{\sigma^{\rm fitted}_{f,iv_i}(E_{\rm in}) - \sigma_{f,iv_i}(E_{\rm in})}{\sigma_{f,iv_i}(E_{\rm in})} \right|, \qquad \sigma_{f,iv_i} = \sum_{v_f} \sigma_{fv_f,iv_i}. \quad (13)$$

To provide an error estimate independent of energy we calculate the weighted root-mean-square error

$$u^{\rm fit}_{f,iv_i} = \sqrt{\sum_{E_{\rm in}} w_{f,iv_i}(E_{\rm in}) \left[u^{\rm fit}_{f,iv_i}(E_{\rm in}) \right]^2}, \quad (14)$$

where the sum is over the energies at which the numerical cross sections have been calculated, and the weights

$$w_{f,iv_i}(E_{\rm in}) = \frac{\sigma_{f,iv_i}(E_{\rm in})}{\sum_{E_{\rm in}} \sigma_{f,iv_i}(E_{\rm in})} \quad (15)$$

ensure that errors near the cross-section maximum are given greater significance than errors where the cross section is small. The errors obtained from Eq. (14) are less than 3% for almost all transitions, and only as large as 5% for some of the transitions with smaller cross sections. Rather than providing error estimates for every transition we choose an overall error of 5%, giving the total uncertainty in the fitted cross sections as $\sqrt{[10\%]^2 + [5\%]^2} = 12\%$ (rounded to the nearest percent). In order to assess the accuracy of the fits at near-threshold energies we also performed the above analysis with the sum in Eq. (14) restricted to energies within 5 eV of the excitation threshold, and found that the errors in this region are still within 5% for almost all transitions.

5. Accessing the data

The cross sections for excitation of bound vibrational levels are provided in supplementary data files named in the format

`MCCC-el-H2-[f]_vf=[vf]_X1Sg_vi=[vi].txt`

where `[f]` is the final electronic-state label (see Appendix A for details on representing the molecular state labels in alphanumeric form), `[vf]` is the final vibrational level in the state `[f]`, and `[vi]` is the initial vibrational level in the $X\ ^1\Sigma_g^+$ state (`[vi]` $= 0, \ldots, 14$).

For example, the file containing the $X\ ^1\Sigma_g^+(v_i = 0) \rightarrow B\ ^1\Sigma_u^+(v_f = 10)$ cross section is named

`MCCC-el-H2-B1Su_vf=10.X1Sg_vi=0.txt`.

Cross sections for DE, cross sections summed over final bound vibrational levels, and cross sections summed over all final levels (including DE) are provided in files named in the format

`MCCC-el-H2-[f]_DE.X1Sg_vi=[vi].txt`
`MCCC-el-H2-[f]_bound.X1Sg_vi=[vi].txt`
`MCCC-el-H2-[f]_total.X1Sg_vi=[vi].txt`.

An example of the data-file format for the $X\ ^1\Sigma_g^+(v_i = 0) \rightarrow B'\ ^1\Sigma_u^+$(DE) cross section is provided in Fig. 6.

The fitting parameters are provided as supplementary data files named in the format

Please cite this article in press as: L.H. Scarlett, D.V. Fursa, M.C. Zammit et al., Complete collision data set for electrons scattering on molecular hydrogen and its isotopologues: I. Fully vibrationally-resolved electronic excitation of $H_2(X\ ^1\Sigma_g^+)$, Atomic Data and Nuclear Data Tables (2020) 101361, https://doi.org/10.1016/j.adt.2020.101361.

```
# Analytic fits to MCCC calculations of electron scattering on molecular hydrogen
# Adiabatic nuclei calculations performed with the spheroidal MCCC(210) model
# Reference:  Scarlett et al.  Atom.  Data Nucl.  Data Tables (2020)
# MCCC Database:  mccc-db.org
# This file:  e + H2(X1Sg,vi=0) -> e + H2(C1Pu) all bound vf + dissociative excitation (DE)
#
# Fitting function:  |(x-1)/x * (a0^2*log(x)/x + a1/x + a2/x^2 + a3/x^3 + a4/x^4 + a5/x^5)|
# where x = energy / threshold_energy
# Yields integrated cross section in atomic units

# vf    vi  threshold (eV)   a0            a1            a2            a3            a4            a5
   0 <-  0  1.22910E+01    7.31110E-01   9.61730E-01  -5.83740E+00   1.34050E+01  -1.31120E+01   4.76360E+00
   1 <-  0  1.25773E+01    8.79090E-01   1.44100E+00  -8.56530E+00   1.94770E+01  -1.89880E+01   6.90670E+00
   2 <-  0  1.28470E+01    8.53080E-01   1.25670E+00  -7.45910E+00   1.68330E+01  -1.62570E+01   5.87210E+00
   3 <-  0  1.31004E+01    7.57640E-01   8.46580E-01  -5.11160E+00   1.15130E+01  -1.10130E+01   3.94420E+00
   4 <-  0  1.33377E+01    6.45970E-01   4.77520E-01  -3.01200E+00   6.79390E+00  -6.38540E+00   2.23880E+00
   5 <-  0  1.35590E+01    5.36480E-01   2.42830E-01  -1.64820E+00   3.75100E+00  -3.46210E+00   1.18270E+00
   6 <-  0  1.37641E+01    4.39720E-01   1.11210E-01  -8.53100E-01   1.96740E+00  -1.76370E+00   5.74650E-01
   7 <-  0  1.39529E+01    3.56330E-01   4.91110E-02  -4.45430E-01   1.04970E+00  -9.19830E-01   2.86540E-01
   8 <-  0  1.41246E+01    2.87770E-01   2.00700E-02  -2.32710E-01   5.60180E-01  -4.74510E-01   1.37640E-01
   9 <-  0  1.42785E+01    2.31470E-01   8.47860E-03  -1.28540E-01   3.15340E-01  -2.60810E-01   7.13580E-02
  10 <-  0  1.44133E+01    1.85400E-01   4.33510E-03  -7.66290E-02   1.89850E-01  -1.56100E-01   4.18850E-02
  11 <-  0  1.45270E+01    1.47450E-01   2.66940E-03  -4.74240E-02   1.16980E-01  -9.55770E-02   2.52700E-02
  12 <-  0  1.46166E+01    1.14370E-01   1.85220E-03  -2.91870E-02   7.10170E-02  -5.78700E-02   1.52680E-02
  13 <-  0  1.46771E+01    7.97590E-02   1.07220E-03  -1.47870E-02   3.54720E-02  -2.89470E-02   7.70000E-03
  DE <-  0  1.46815E+01    2.10230E-01   6.68100E-02  -3.59840E-01   7.21910E-01  -6.02840E-01   1.74370E-01
```

Fig. 7. The format of the file `MCCC-el-H2-C1Pu.X1Sg_vi=0_fit.txt`, containing cross-section fitting parameters for excitation of each level in the $C\ ^1\Pi_u$ state from the $v_i = 0$ level of the $X\ ^1\Sigma_g^+$ state of H_2. Each line corresponds to a vibrational level v_f in the excited electronic state and specifies the excitation energy and each of the fitting parameters for the given transition. The final line provides the fitting parameters for the dissociative-excitation (DE) cross section.

`MCCC-el-H2-[f].X1Sg_vi=[vi]_fit.txt`.

An example of the fitting-parameter file for the $C\ ^1\Pi_u$ state and $v_i = 0$ is given in Fig. 7.

The present set of cross sections can also be downloaded from the MCCC database website at http://mccc-db.org. This repository will be continuously updated as new results are produced and is the best location to access the entire database of MCCC cross sections.

6. Conclusions

We have presented a comprehensive set of fully vibrationally-resolved cross sections for electrons scattering on the vibrationally-excited ground state of H_2. Analytic fits have been provided for all transitions, and we have estimated an uncertainty of 10% in the numerical data and 12% in the fitted data. All numerical and fitted results are available as supplementary data files. The present calculations represent a substantial improvement over the previously available data for electron–H_2 collisions, in both quality and quantity, and we hope they will be of use in plasma-modeling applications. Future contributions to the dataset will include cross sections for rovibrational excitation, viscosity and momentum transfer, ionization, and dissociation for each of the isotopologues of H_2.

Declaration of competing interest

The authors declare that they have no known competing financial interests or personal relationships that could have appeared to influence the work reported in this paper.

Acknowledgment

We are grateful to Dr. D. Wünderlich for useful discussions surrounding the applications of the present results, and Dr. C. J. Fontes for providing helpful feedback on the manuscript. This work was supported by the United States Air Force Office of Scientific Research, Curtin University, Los Alamos National Laboratory (LANL), and resources provided by the Pawsey Supercomputing Centre, with funding from the Australian Government and Government of Western Australia. L.H.S. acknowledges the contribution of an Australian Government Research Training Program Scholarship, and the support of the Forrest Research Foundation. M.C.Z. would like to specifically acknowledge LANL's ASC PEM Atomic Physics Project for its support. LANL is operated by Triad National Security, LLC, for the National Nuclear Security Administration of the U.S. Department of Energy under Contract No. 89233218NCA000001.

Appendix A. Diatomic state notation

In this paper we utilize the standard diatomic electronic-state notation (as used by Sharp [47], for example) which we briefly describe here. The symmetry properties of a state are specified by a label in the form

$$^{2s+1}\Lambda_{u/g},$$

where s is the total electronic spin, Λ is the magnitude of the electronic orbital angular momentum projection along the internuclear axis, and u/g refer to the *ungerade* (odd) or *gerade* (even) parities of the orbital angular momentum. The value of Λ is specified by a capital Greek letter which follows a similar rule to the s, p, d, f convention of atomic orbitals (Σ, Π, Δ,

Φ, etc.). For example, the ground electronic state ($X\ ^1\Sigma_g^+$) has $s = 0$, $\Lambda = 0$, and even electronic parity. The $+$ $(-)$ superscript on the Σ states indicates that the electronic state is symmetric (antisymmetric) under reflection through a plane containing the internuclear axis. The symmetry labels are prefaced by Latin letters to uniquely specify the electronic states. The ground electronic state is given the "X" label. States of the same spin as the ground state are assigned upper-case letters while states of different spin are assigned lower-case letters. A number of states which were initially considered separate based on spectroscopic measurements have been subsequently identified as double-minima states and assigned a conjoined state label (e.g. $E\ ^1\Sigma_g^+ + F\ ^1\Sigma_g^+ \rightarrow EF\ ^1\Sigma_g^+$) [47]. States which were initially identified as double-minima states are assigned a single-character label as usual, but some authors prefer to retain the double-character notation by repeating the letter with a bar, (e.g. $H\bar{H}\ ^1\Sigma_g^+$). For simplicity of converting state labels to alphanumeric strings for file-naming purposes we follow the convention of Sharp [47] which is to specify these states by the single letter only. When converting state labels to alphanumeric form we replace the capital Greek letter by the corresponding capital Latin letter, and primes on the Latin letters are replaced by a p. For example:

$H\ ^1\Sigma_g^+ \rightarrow$ H1Sg

$b\ ^3\Sigma_u^+ \rightarrow$ b3Su

$B'\ ^1\Sigma_u^+ \rightarrow$ Bp1Su.

Appendix B. Supplementary data

Supplementary material related to this article can be found online at https://doi.org/10.1016/j.adt.2020.101361.

References

[1] A. Bhardwaj, G.R. Gladstone, Rev. Geophys. 38 (2000) 295.
[2] C. Tao, S.V. Badman, M. Fujimoto, Icarus 213 (2011) 581.
[3] D. Wünderlich, U. Fantz, Atoms 4 (2016) 26.
[4] K. Sawada, T. Fujimoto, J. Appl. Phys. 78 (1995) 2913.
[5] S.I. Krasheninnikov, A.Y. Pigarov, D.J. Sigmar, Contrib. Plasma Phys. 36 (1996) 314, (ISSN: 08631042).
[6] S.I. Krasheninnikov, A.S. Kukushkin, A.A. Pshenov, Phys. Plasmas 23 (2016) (ISSN: 10897674).
[7] U. Fantz, P. Franzen, W. Kraus, M. Berger, S. Christ-Koch, H. Falter, M. Fröschle, R. Gutser, B. Heinemann, C. Martens, et al., Nucl. Fusion 49 (2009) 125007.
[8] Yu. Ralchenko, Modern Methods of Radiative Modeling in Plasmas, Springer, 2016.
[9] G.J. Hagelaar, L.C. Pitchford, Plasma Sources. Sci. Technol. 14 (2005) 722.
[10] D.H. Sampson, H.L. Zhang, C.J. Fontes, Phys. Rep. 477 (2009) 111.
[11] M.F. Gu, Can. J. Phys. 86 (2008) 675.
[12] C. Fontes, H. Zhang, J. Abdalla Jr., R. Clark, D. Kilcrease, J. Colgan, R. Cunningham, P. Hakel, N. Magee, M. Sherrill, J. Phys. B: At. Mol. Opt. Phys. 48 (2015) 144014.
[13] H.-K. Chung, M.H. Chen, W.L. Morgan, Yu. Ralchenko, R.W. Lee, High Energy Density Phys. 1 (2005) 3.
[14] H.-K. Chung, C. Bowen, C.J. Fontes, S.B. Hansen, Yu. Ralchenko, High Energy Density Phys. 9 (2013) 645.
[15] R. Piron, F. Gilleron, Y. Aglitskiy, H.-K. Chung, C.J. Fontes, S.B. Hansen, O. Marchuk, H.A. Scott, E. Stambulchik, Yu. Ralchenko, High Energy Density Phys. 23 (2017) 38.
[16] D. Wünderlich, S. Dietrich, U. Fantz, J. Quant. Spectrosc. Radiat. Transfer 110 (2009) 62.
[17] M. Goto, J. Quant. Spectrosc. Radiat. Transfer 76 (2003) 331.
[18] K. Kano, M. Suzuki, H. Akatsuka, Contrib. Plasma Phys. 41 (2001) 91.
[19] Dipti, T. Das, K. Bartschat, I. Bray, D.V. Fursa, O. Zatsarinny, C. Ballance, H.K. Chung, Yu. Ralchenko, At. Data Nucl. Data Tables 127–128 (2019) 1.
[20] R.K. Janev, D. Reiter, U. Samm, Sci. York (2003) 190.
[21] W.T. Miles, R. Thompson, A.E.S. Green, J. Appl. Phys. 43 (1972) 678.
[22] J.-S. Yoon, Y.-W. Kim, D.-C. Kwon, M.-Y. Song, W.-S. Chang, C.-G. Kim, V. Kumar, B. Lee, Phys. Rep. 73 (2010) 116401.
[23] R. Celiberto, R. Janev, A. Laricchiuta, M. Capitelli, J. Wadehra, D. Atems, At. Data Nucl. Data Tables 77 (2001) 161.
[24] J.K. Tapley, L.H. Scarlett, J.S. Savage, M.C. Zammit, D.V. Fursa, I. Bray, J. Phys. B: At. Mol. Phys. (ISSN: 2190-4995) 51 (2018) 144007.
[25] M.C. Zammit, J.S. Savage, D.V. Fursa, I. Bray, Phys. Rev. A 952 (2017) 022708.
[26] M. Zawadzki, R. Wright, G. Dolmat, M.F. Martin, L. Hargeaves, D.V. Fursa, M.C. Zammit, L.H. Scarlett, J.K. Tapley, J.S. Savage, et al., Phys. Rev. A 97 (2018) 050702(R).
[27] M. Zawadzki, R. Wright, G. Dolmat, M.F. Martin, B. Diaz, L. Hargreaves, D. Coleman, D.V. Fursa, M.C. Zammit, L.H. Scarlett, et al., Phys. Rev. A 98 (2018) 062704.
[28] L.H. Scarlett, J.S. Savage, D.V. Fursa, I. Bray, M.C. Zammit, Eur. Phys. J. D 74 (2020) 36.
[29] J.K. Tapley, L.H. Scarlett, J.S. Savage, D.V. Fursa, M.C. Zammit, I. Bray, Phys. Rev. A 98 (2018) 032701.
[30] L.H. Scarlett, J.K. Tapley, J.S. Savage, D.V. Fursa, M.C. Zammit, I. Bray, Plasma Sources. Sci. Technol. 28 (2019) 025004.
[31] L.H. Scarlett, J.S. Savage, D.V. Fursa, M.C. Zammit, I. Bray, Atoms 7 (2019) 75.
[32] W. Kolos, K. Szalewicz, H.J. Monkhorst, J. Chem. Phys. 84 (1986) 3278.
[33] G. Staszewska, L. Wolniewicz, J. Mol. Spectrosc. 212 (2002) 208.
[34] L. Wolniewicz, K. Dressler, J. Chem. Phys. 100 (1994) 444.
[35] L. Wolniewicz, G. Staszewska, J. Mol. Spectrosc. 220 (2003) 45.
[36] L. Wolniewicz, J. Mol. Spectrosc. 169 (1995) 329.
[37] G. Staszewska, L. Wolniewicz, J. Mol. Spectrosc. 198 (1999) 416.
[38] J. Brown, A. Carrington, Rotational Spectroscopy of Diatomic Molecules, Cambridge University Press, Cambridge, 2003.
[39] U. Fantz, D. Wünderlich, At. Data Nucl. Data Tables 92 (2006) 853.
[40] S.C. Ross, T. Yoshinari, Y. Ogi, K. Tsukiyama, J. Chem. Phys. 125 (2006) 133205.
[41] M.C. Zammit, D.V. Fursa, J.S. Savage, I. Bray, J. Phys. B: At. Mol. Opt. Phys. 50 (2017) 123001.
[42] L.H. Scarlett, M.C. Zammit, D.V. Fursa, I. Bray, Phys. Rev. A 96 (2017) 022706.
[43] M.C. Zammit, D.V. Fursa, J.S. Savage, L. Chiari, A. Zecca, M.J. Brunger, Phys. Rev. 95 (2017) 022707.
[44] L.H. Scarlett, J.K. Tapley, D.V. Fursa, M.C. Zammit, J.S. Savage, I. Bray, Phys. Rev. A 96 (2017) 062708.
[45] M. Shugard, A.U. Hazi, Phys. Rev. A 12 (1975) 1895.
[46] D.T. Stibbe, J. Tennyson, New J. Phys. 1 (1998) 2.
[47] T.E. Sharp, At. Data Nucl. Data Tables 2 (1971) 119.

Please cite this article in press as: L.H. Scarlett, D.V. Fursa, M.C. Zammit et al., Complete collision data set for electrons scattering on molecular hydrogen and its isotopologues: I. Fully vibrationally-resolved electronic excitation of $H_2(X\ ^1\Sigma_g^+)$, Atomic Data and Nuclear Data Tables (2020) 101361, https://doi.org/10.1016/j.adt.2020.101361.

Explanation of tables

Table 1. Vibrational-state energies.

Energies (in Hartrees) are given for a maximum of 15 vibrational levels in each electronic state. Vibrational levels with wave functions located in the outer well of a double-minima state are marked with an asterisk. A dash indicates a level which is not present in the calculations of Ref. [39].

v	Vibrational quantum number
E_v	Energy of the vibrational level v in an electronic state
Ref. [39]	Energies from the calculations of Fantz and Wünderlich [39] for comparison

Please cite this article in press as: L.H. Scarlett, D.V. Fursa, M.C. Zammit et al., Complete collision data set for electrons scattering on molecular hydrogen and its isotopologues: I. Fully vibrationally-resolved electronic excitation of $H_2(X\ ^1\Sigma_g^+)$, Atomic Data and Nuclear Data Tables (2020) 101361, https://doi.org/10.1016/j.adt.2020.101361.

Explanation of graphs

Graph 1. Dissociative excitation cross sections.

Electron-impact dissociative excitation of the $B\ ^1\Sigma_u^+$, $C\ ^1\Pi_u$, $B'\ ^1\Sigma_u^+$, $b\ ^3\Sigma_u^+$, $a\ ^3\Sigma_g^+$, and $c\ ^3\Pi_u$ states from the $X\ ^1\Sigma_g^+$ state of H_2.

v_i Initial vibrational level in the $X\ ^1\Sigma_g^+$ state

Graph 2. Bound excitation cross sections for the $B\ ^1\Sigma_u^+$ state.

Graph 3. Bound excitation cross sections for the $C\ ^1\Pi_u$ state.

Graph 4. Bound excitation cross sections for the $B'\ ^1\Sigma_u^+$ state.

Graph 5. Bound excitation cross sections for the $a\ ^3\Sigma_g^+$ state.

Graph 6. Bound excitation cross sections for the $c\ ^3\Pi_u$ state.

Graph 7. Bound excitation cross sections for the $d\ ^3\Pi_u$ state.

Electron-impact excitation of a selection of bound vibrational levels in the $B\ ^1\Sigma_u^+$, $C\ ^1\Pi_u$, $B'\ ^1\Sigma_u^+$, $a\ ^3\Sigma_g^+$, $c\ ^3\Pi_u$, and $d\ ^3\Pi_u$ states from the $X\ ^1\Sigma_g^+$ state of H_2. Each line represents a different vibrational level in the excited electronic state.

v_i Initial vibrational level in the $X\ ^1\Sigma_g^+$ state

v_f Final vibrational level in the excited electronic state

Please cite this article in press as: L.H. Scarlett, D.V. Fursa, M.C. Zammit et al., Complete collision data set for electrons scattering on molecular hydrogen and its isotopologues: I. Fully vibrationally-resolved electronic excitation of $H_2(X\ ^1\Sigma_g^+)$, Atomic Data and Nuclear Data Tables (2020) 101361, https://doi.org/10.1016/j.adt.2020.101361.

Table 1
Vibrational-state energies. See explanation of tables.

v	$X\ ^1\Sigma_g^+$		$B\ ^1\Sigma_u^+$		$C\ ^1\Pi_u$		$EF\ ^1\Sigma_g^+$		$B'\ ^1\Sigma_u^+$	
	E_v	Ref. [39]	E_v	Ref. [39]	E_v	Ref. [39]	E_v	Ref. [39]	E_v	Ref. [39]
0	−1.1645	−1.1644	−0.7536	−0.7536	−0.7128	−0.7128	−0.7125	−0.7125	−0.6612	−0.6612
1	−1.1456	−1.1454	−0.7476	−0.7475	−0.7023	−0.7023	−0.7117*	−0.7117*	−0.6526	−0.6526
2	−1.1277	−1.1275	−0.7417	−0.7417	−0.6924	−0.6924	−0.7063*	−0.7063*	−0.6448	−0.6448
3	−1.1108	−1.1107	−0.7360	−0.7360	−0.6831	−0.6831	−0.7019	−0.7019	−0.6378	−0.6378
4	−1.0950	−1.0948	−0.7305	−0.7305	−0.6744	−0.6744	−0.7011*	−0.7011*	−0.6318	−0.6318
5	−1.0802	−1.0801	−0.7251	−0.7251	−0.6663	−0.6662	−0.6962*	−0.6962*	−0.6274	−0.6274
6	−1.0665	−1.0664	−0.7198	−0.7198	−0.6587	−0.6587	−0.6927	−0.6927	−0.6260	−0.6260
7	−1.0538	−1.0537	−0.7147	−0.7147	−0.6518	−0.6518	−0.6913*	−0.6913*	−0.6255	−0.6255
8	−1.0423	−1.0421	−0.7098	−0.7098	−0.6455	−0.6455	−0.6874	−0.6874	−0.6252	−0.6252
9	−1.0318	−1.0317	−0.7050	−0.7050	−0.6398	−0.6398	−0.6843	−0.6843	−0.6250	–
10	−1.0226	−1.0225	−0.7003	−0.7003	−0.6349	−0.6349	−0.6815	−0.6815		
11	−1.0147	−1.0146	−0.6958	−0.6958	−0.6307	−0.6307	−0.6781	−0.6781		
12	−1.0082	−1.0082	−0.6914	−0.6914	−0.6274	−0.6274	−0.6748	−0.6749		
13	−1.0035	−1.0035	−0.6872	−0.6872	−0.6252	−0.6252	−0.6717	−0.6717		
14	−1.0006	−1.0007	−0.6830	−0.6830			−0.6685	−0.6685		

v	$GK\ ^1\Sigma_g^+$		$I\ ^1\Pi_g$		$J\ ^1\Delta_g$		$D\ ^1\Pi_u$		$H\ ^1\Sigma_g^+$	
	E_v	Ref. [39]	E_v	Ref. [39]	E_v	Ref. [39]	E_v	Ref. [39]	E_v	Ref. [39]
0	−0.6578*	−0.6577*	−0.6544	−0.6544	−0.6523	−0.6523	−0.6500	−0.6500	−0.6496	−0.6496
1	−0.6557	−0.6557	−0.6448	−0.6448	−0.6422	−0.6422	−0.6399	−0.6398	−0.6395	−0.6395
2	−0.6494	−0.6494	−0.6359	−0.6359	−0.6326	−0.6327	−0.6303	−0.6303	−0.6304	−0.6303
3	−0.6456	−0.6456	−0.6278	−0.6278	−0.6238	−0.6237	−0.6213	−0.6213	−0.6224	−0.6224
4	−0.6404	−0.6404	−0.6256*	–	−0.6154	−0.6153	−0.6129	−0.6129	−0.6150	−0.6150
5	−0.6357	−0.6357	−0.6252*	–	−0.6075	−0.6075	−0.6050	−0.6050	−0.6081	−0.6081
6	−0.6314	−0.6314	−0.6251*	–	−0.6001	−0.6001	−0.5977	−0.5977	−0.6046*	−0.6045*
7	−0.6278	−0.6278	−0.6250*	–	−0.5933	−0.5933	−0.5909	−0.5909	−0.6029*	−0.6029*
8	−0.6253	−0.6253	−0.6250*	–	−0.5870	−0.5870	−0.5847	−0.5847	−0.6017	−0.6017*
9					−0.5812	−0.5811	−0.5790	−0.5790	−0.6013*	−0.6013*
10					−0.5759	−0.5759	−0.5738	−0.5738	−0.5997*	−0.5998*
11					−0.5711	−0.5711	−0.5693	−0.5693	−0.5983*	−0.5984*
12					−0.5669	−0.5669	−0.5653	−0.5653	−0.5968*	−0.5969*
13					−0.5633	−0.5633	−0.5620	−0.5620	−0.5960	−0.5959*
14					−0.5603	−0.5603	−0.5593	−0.5593	−0.5955*	−0.5955*

v	$a\ ^3\Sigma_g^+$		$c\ ^3\Pi_u$		$d\ ^3\Pi_u$		$g\ ^3\Sigma_g^+$		$j\ ^3\Delta_g$	
	E_v	Ref. [39]	E_v	Ref. [39]	E_v	Ref. [39]	E_v	Ref. [39]	E_v	Ref. [39]
0	−0.7311	−0.7311	−0.7320	−0.7319	−0.6554	−0.6553	−0.6542	−0.6541	−0.6523	−0.6523
1	−0.7196	−0.7196	−0.7213	−0.7213	−0.6451	−0.6451	−0.6435	−0.6435	−0.6422	−0.6422
2	−0.7087	−0.7087	−0.7112	−0.7112	−0.6355	−0.6355	−0.6336	−0.6336	−0.6327	−0.6327
3	−0.6985	−0.6984	−0.7016	−0.7016	−0.6264	−0.6264	−0.6243	−0.6243	−0.6238	−0.6238
4	−0.6888	−0.6887	−0.6926	−0.6926	−0.6178	−0.6178	−0.6156	−0.6155	−0.6154	−0.6154
5	−0.6796	−0.6796	−0.6841	−0.6840	−0.6098	−0.6098	−0.6074	−0.6073	−0.6075	−0.6075
6	−0.6711	−0.6711	−0.6761	−0.6760	−0.6023	−0.6023	−0.5997	−0.5997	−0.6002	−0.6002
7	−0.6632	−0.6631	−0.6686	−0.6685	−0.5953	−0.5953	−0.5927	−0.5926	−0.5934	−0.5934
8	−0.6558	−0.6558	−0.6616	−0.6616	−0.5888	−0.5888	−0.5861	−0.5861	−0.5870	−0.5870
9	−0.6491	−0.6491	−0.6551	−0.6551	−0.5828	−0.5828	−0.5801	−0.5801	−0.5812	−0.5812
10	−0.6430	−0.6430	−0.6492	−0.6492	−0.5773	−0.5774	−0.5747	−0.5747	−0.5759	−0.5759
11	−0.6377	−0.6377	−0.6439	−0.6439	−0.5724	−0.5724	−0.5700	−0.5700	−0.5712	−0.5712
12	−0.6331	−0.6332	−0.6391	−0.6391	−0.5681	−0.5681	−0.5660	−0.5660	−0.5670	−0.5670
13	−0.6296	−0.6296	−0.6350	−0.6350	−0.5643	−0.5643	−0.5628	−0.5629	−0.5633	−0.5634
14	−0.6272	−0.6272	−0.6315	−0.6316	−0.5612	−0.5612	−0.5604	−0.5604	−0.5603	−0.5604

v	$e\ ^3\Sigma_u^+$		$h\ ^3\Sigma_g^+$		$i\ ^3\Pi_g$	
	E_v	Ref. [39]	E_v	Ref. [39]	E_v	Ref. [39]
0	−0.6785	−0.6785	−0.6558	−0.6558	−0.6545	−0.6544
1	−0.6691	−0.6690	−0.6466	−0.6466	−0.6448	−0.6448
2	−0.6603	−0.6603	−0.6380	−0.6379	−0.6358	−0.6358
3	−0.6521	−0.6521	−0.6300	−0.6300	−0.6275	−0.6275
4	−0.6446	−0.6446				
5	−0.6378	−0.6378				
6	−0.6319	−0.6319				
7	−0.6270	−0.6270				

Please cite this article in press as: L.H. Scarlett, D.V. Fursa, M.C. Zammit et al., Complete collision data set for electrons scattering on molecular hydrogen and its isotopologues: I. Fully vibrationally-resolved electronic excitation of $H_2(X\ ^1\Sigma_g^+)$, Atomic Data and Nuclear Data Tables (2020) 101361, https://doi.org/10.1016/j.adt.2020.101361.

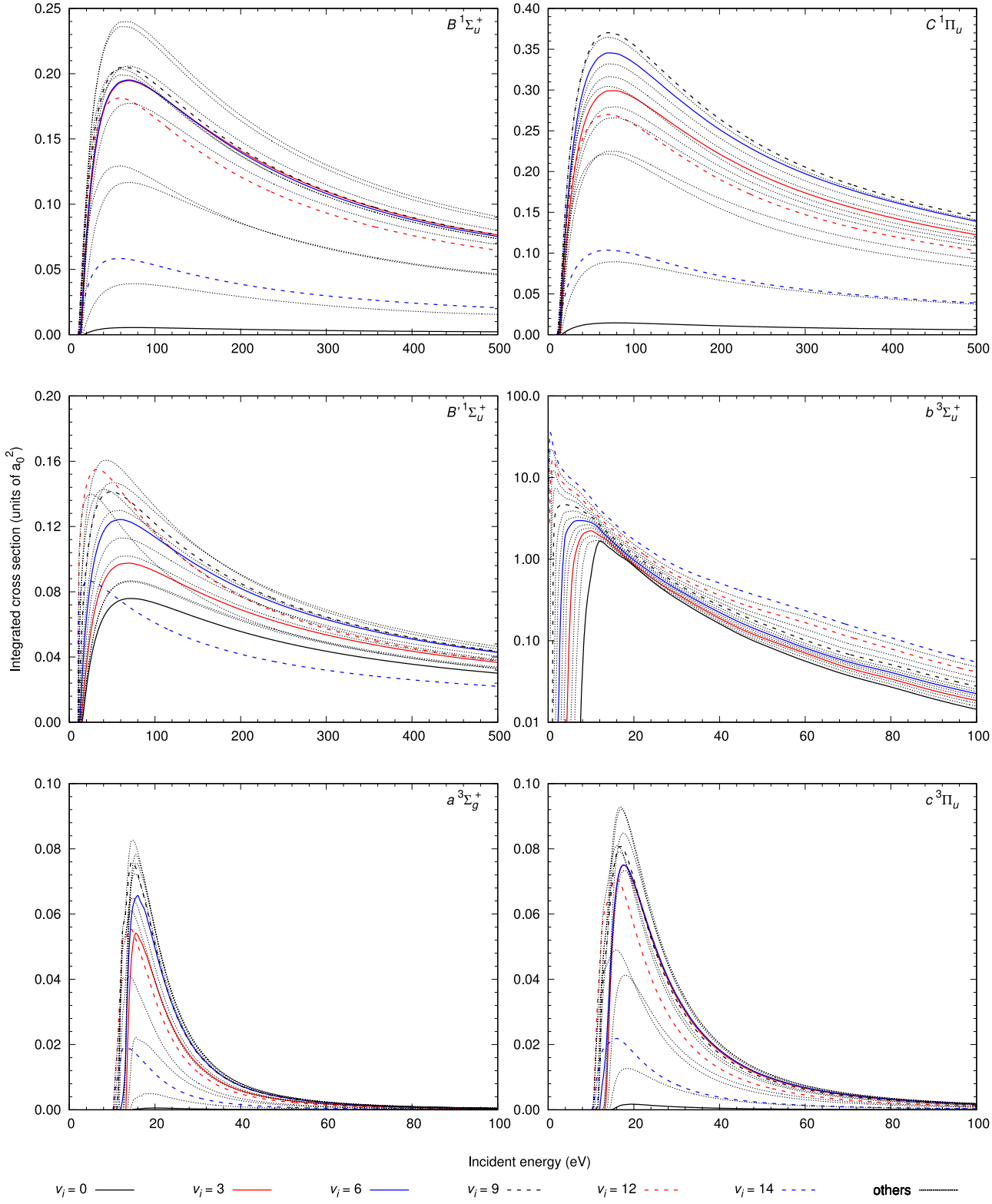

Graph 1. Dissociative excitation cross sections. See Explanation of Graphs.

Please cite this article in press as: L.H. Scarlett, D.V. Fursa, M.C. Zammit et al., Complete collision data set for electrons scattering on molecular hydrogen and its isotopologues: I. Fully vibrationally-resolved electronic excitation of $H_2(X\,^1\Sigma_g^+)$, Atomic Data and Nuclear Data Tables (2020) 101361, https://doi.org/10.1016/j.adt.2020.101361.

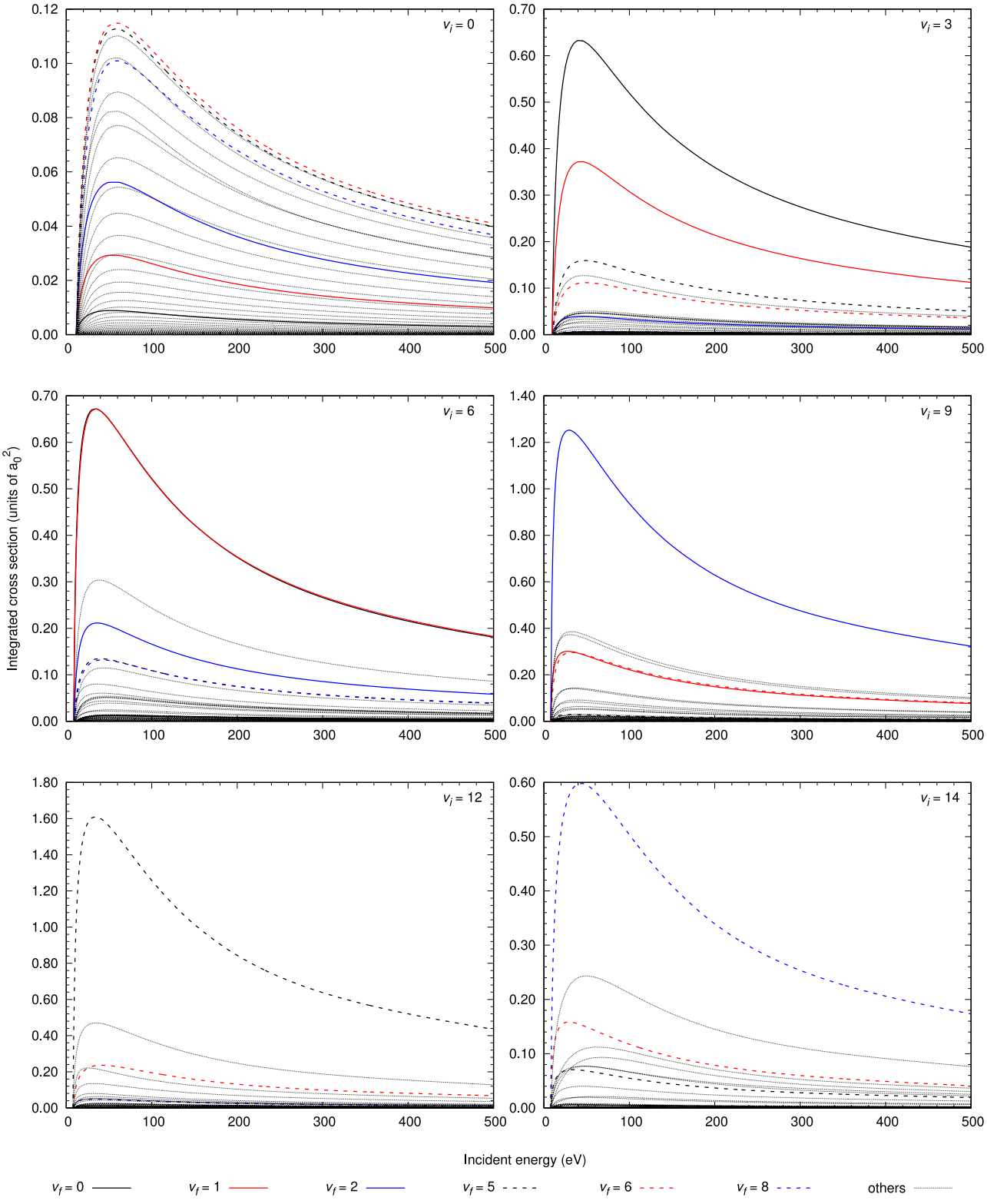

Graph 2. Bound excitation cross sections for the $B\ ^1\Sigma_u^+$ state. See Explanation of Graphs.

Please cite this article in press as: L.H. Scarlett, D.V. Fursa, M.C. Zammit et al., Complete collision data set for electrons scattering on molecular hydrogen and its isotopologues: I. Fully vibrationally-resolved electronic excitation of $H_2(X\ ^1\Sigma_g^+)$, Atomic Data and Nuclear Data Tables (2020) 101361, https://doi.org/10.1016/j.adt.2020.101361.

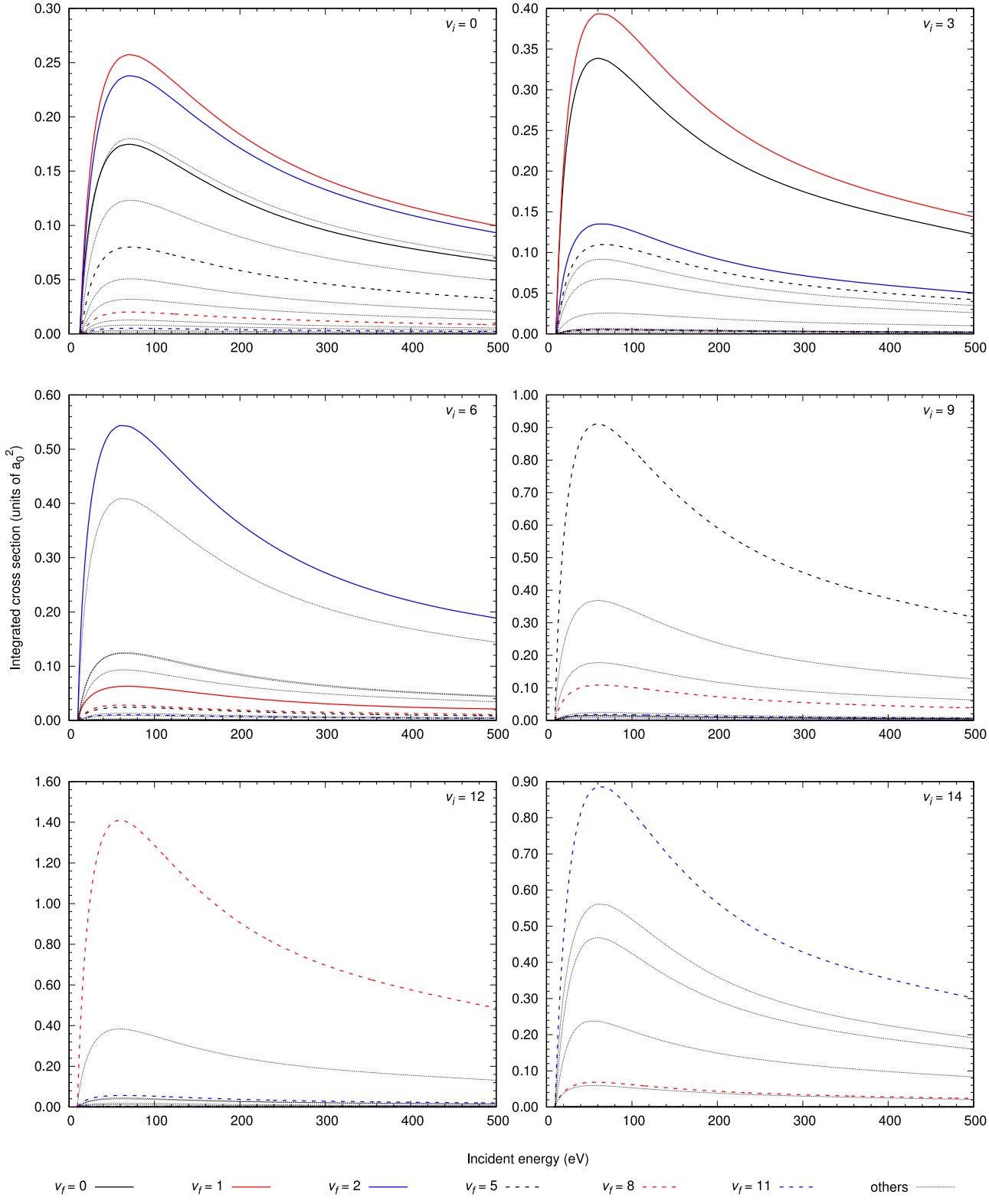

Graph 3. Bound excitation cross sections for the $C\ ^1\Pi_u$ state. See Explanation of Graphs.

Please cite this article in press as: L.H. Scarlett, D.V. Fursa, M.C. Zammit et al., Complete collision data set for electrons scattering on molecular hydrogen and its isotopologues: I. Fully vibrationally-resolved electronic excitation of $H_2(X\ ^1\Sigma_g^+)$, Atomic Data and Nuclear Data Tables (2020) 101361, https://doi.org/10.1016/j.adt.2020.101361.

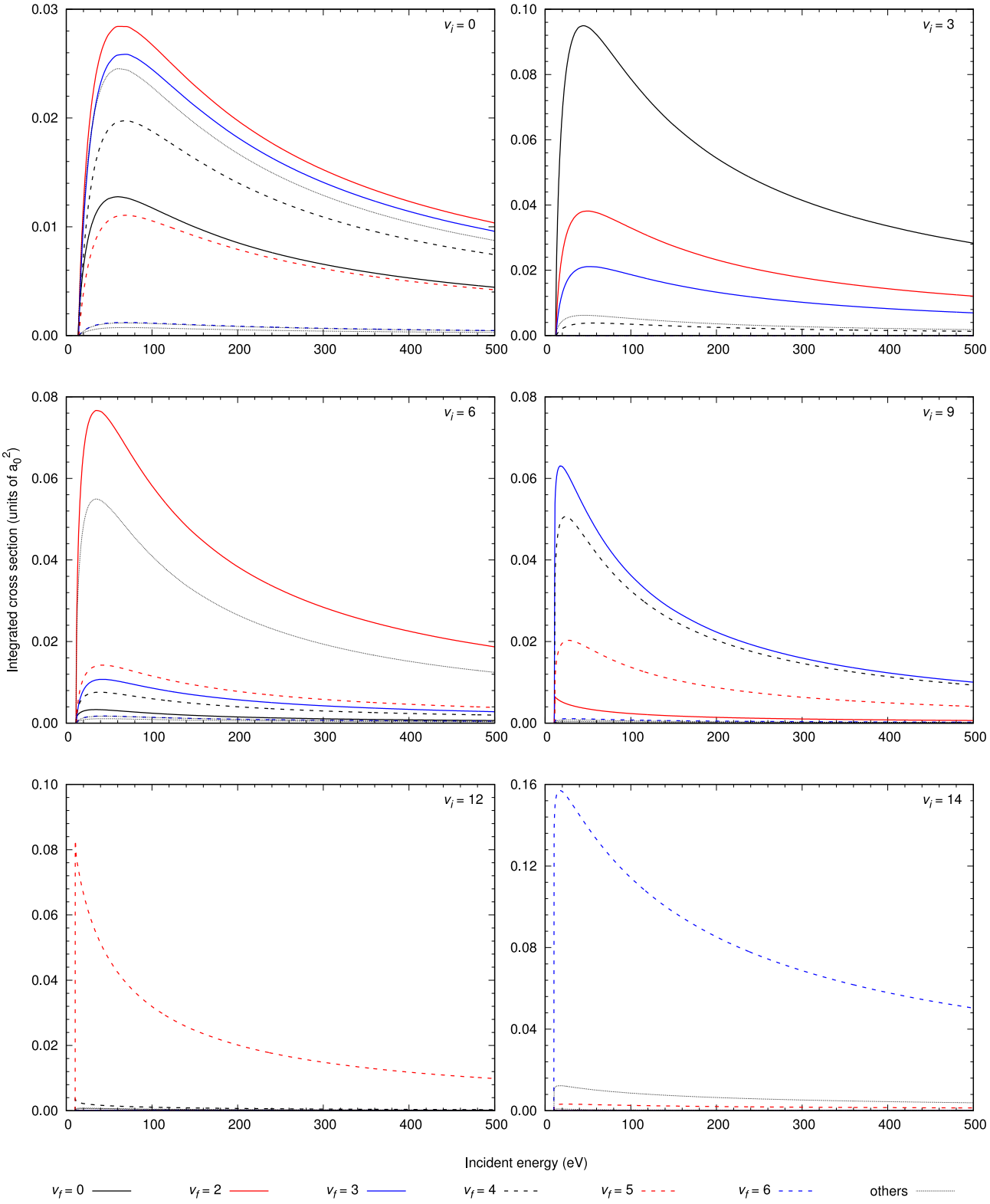

Graph 4. Bound excitation cross sections for the $B'\ ^1\Sigma_u^+$ state. See Explanation of Graphs.

Please cite this article in press as: L.H. Scarlett, D.V. Fursa, M.C. Zammit et al., Complete collision data set for electrons scattering on molecular hydrogen and its isotopologues: I. Fully vibrationally-resolved electronic excitation of $H_2(X\ ^1\Sigma_g^+)$, Atomic Data and Nuclear Data Tables (2020) 101361, https://doi.org/10.1016/j.adt.2020.101361.

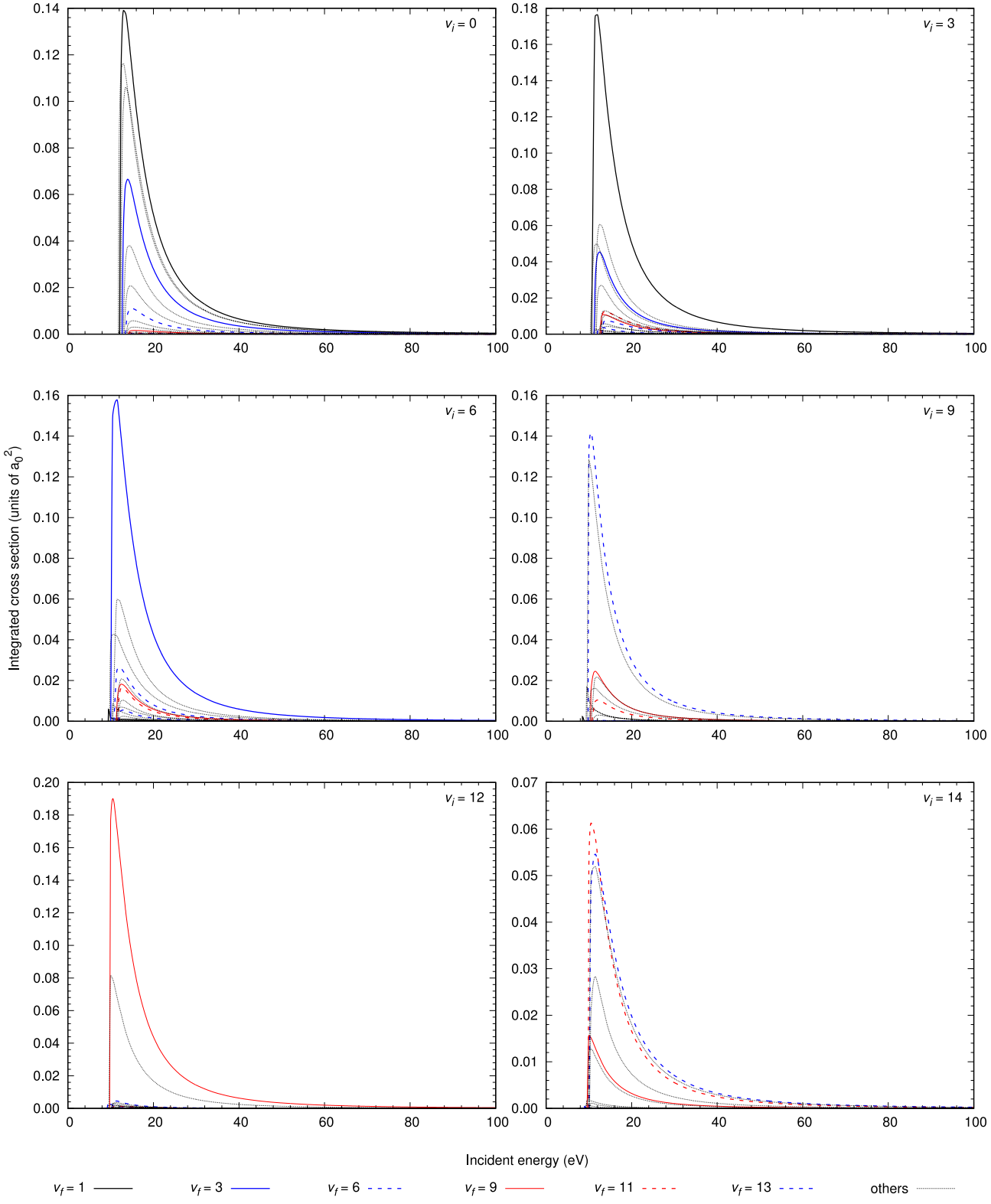

Graph 5. Bound excitation cross sections for the $a\ ^3\Sigma_g^+$ state. See Explanation of Graphs.

Please cite this article in press as: L.H. Scarlett, D.V. Fursa, M.C. Zammit et al., Complete collision data set for electrons scattering on molecular hydrogen and its isotopologues: I. Fully vibrationally-resolved electronic excitation of $H_2(X\ ^1\Sigma_g^+)$, Atomic Data and Nuclear Data Tables (2020) 101361, https://doi.org/10.1016/j.adt.2020.101361.

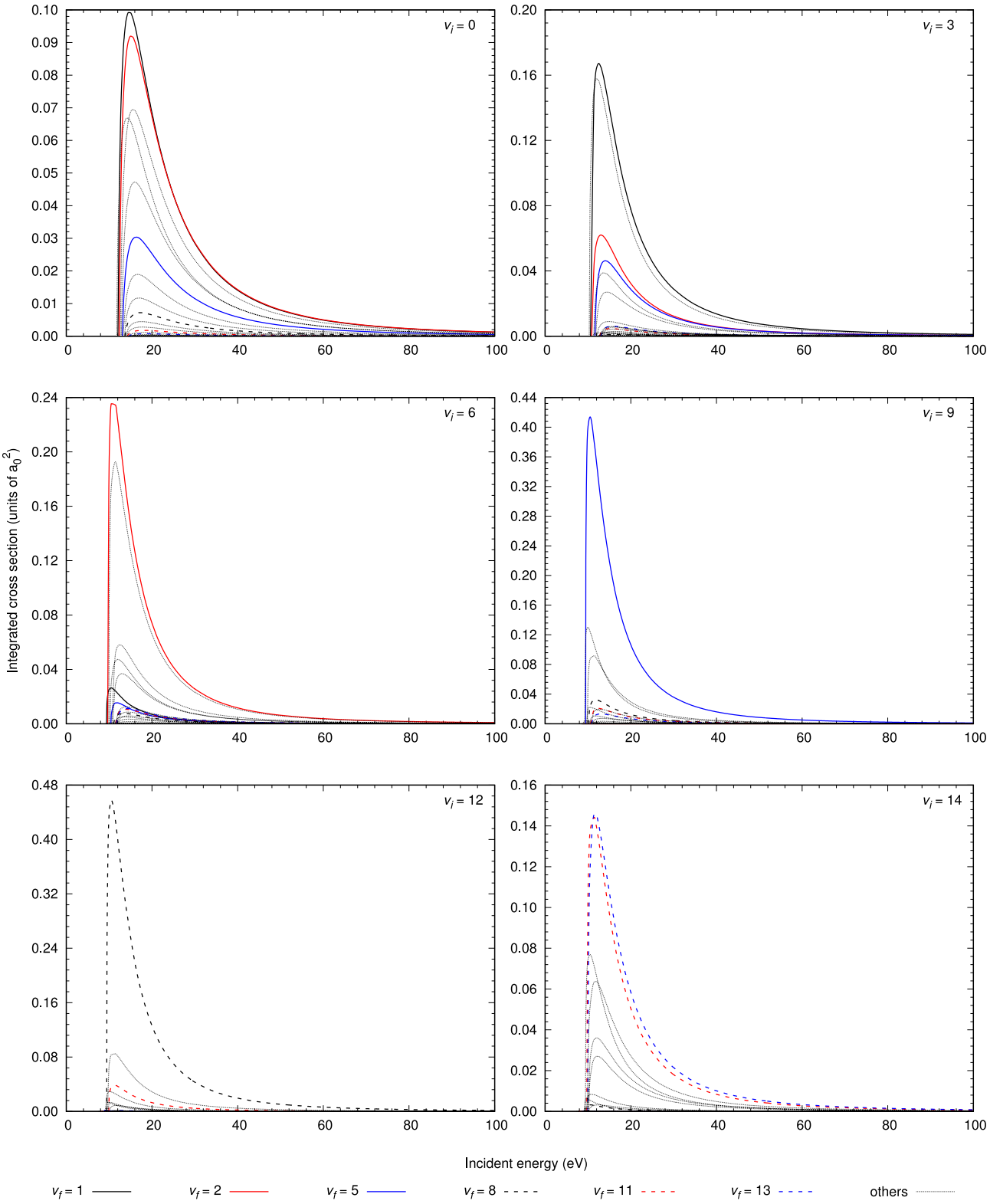

Graph 6. Bound excitation cross sections for the $c\ ^3\Pi_u$ state. See Explanation of Graphs.

Please cite this article in press as: L.H. Scarlett, D.V. Fursa, M.C. Zammit et al., Complete collision data set for electrons scattering on molecular hydrogen and its isotopologues: I. Fully vibrationally-resolved electronic excitation of $H_2(X\ ^1\Sigma_g^+)$, Atomic Data and Nuclear Data Tables (2020) 101361, https://doi.org/10.1016/j.adt.2020.101361.

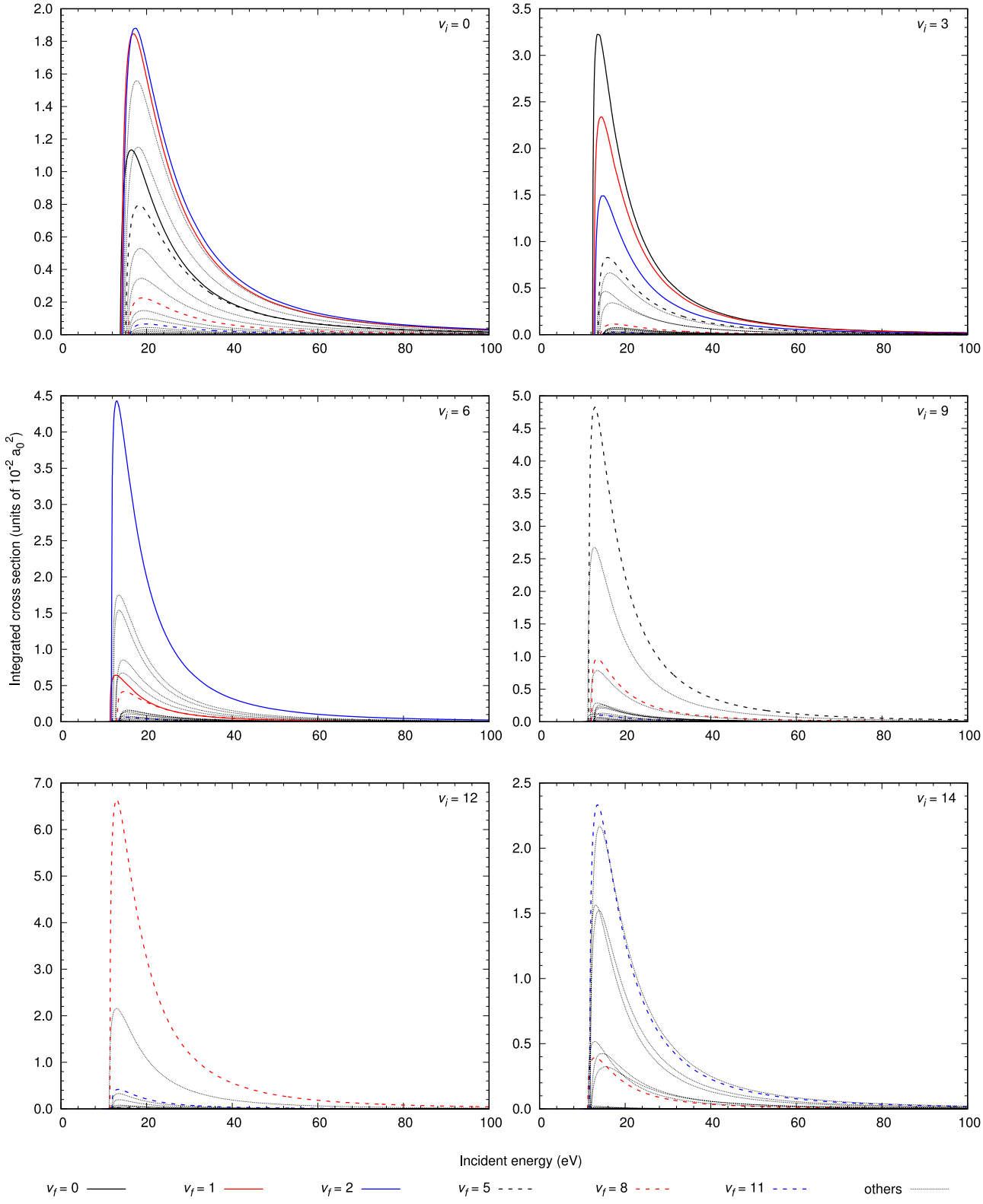

Graph 7. Bound excitation cross sections for the $d\ ^3\Pi_u$ state. See Explanation of Graphs.

Please cite this article in press as: L.H. Scarlett, D.V. Fursa, M.C. Zammit et al., Complete collision data set for electrons scattering on molecular hydrogen and its isotopologues: I. Fully vibrationally-resolved electronic excitation of $H_2(X\ ^1\Sigma_g^+)$, Atomic Data and Nuclear Data Tables (2020) 101361, https://doi.org/10.1016/j.adt.2020.101361.